

Spin-dependent tunneling in the nearly-free-electron model

P. BOSE^{*†}, J. HENK[‡] and I. MERTIG[†]

[†]Martin-Luther-Universität Halle-Wittenberg, Germany

[‡]Max-Planck-Institut für Mikrostrukturphysik, Germany

Short title: Computing tunnel conductances by NFE

Words: 5860

**Corresponding author:*

P. Bose

FB Theoretische Physik, FB Physik

Martin-Luther-Universität Halle-Wittenberg D-06099 Halle (Saale), Germany

Electronic address: bose@physik.uni-halle.de

Telephone: +49 (0)345 5525-460

Fax: +49 (0)345 5525-446

Dr. J. Henk

Max-Planck-Institut für Mikrostrukturphysik

Weinberg 2, D-06120 Halle (Saale), Germany

Electronic address: henk@mpi-halle.de

Telephone: +49 (0)345 5582-970

Fax: +49 (0)345 5582-765

Prof. Dr. I. Mertig

FB Theoretische Physik, FB Physik

Martin-Luther-Universität Halle-Wittenberg D-06099 Halle (Saale), Germany

Electronic address: mertig@physik.uni-halle.de

Telephone: +49 (0)345 5525-430

Fax: +49 (0)345 5525-446

Spin-dependent ballistic transport through a tunnel barrier is treated within the one-dimensional nearly-free-electron model. The comparison with free electrons reveals significant effects of band gaps, in particular in the bias dependence. The results are qualitatively explained by the number of incident and transmitted states in the leads. With an extension to ferromagnetic leads the bias dependence of tunnel magneto-resistance is discussed.

Keywords: Nearly free electrons; Tunneling; Ballistic transport; Bias dependence; Tunnel magneto-resistance;

1. Introduction

Spin-dependent transport of electrons in nanostructures is one of most rapidly evolving areas of contemporary physics [1, 2]. Important contributions to the field come from applied physics, focusing on design and characterization of devices and applications, and from experimental physics, aiming at the understanding of fundamental effects. Contributions from theoretical physics comprise on one hand transport calculations that are based on state-of-the-art electronic-structure calculations. By this means, properties of specific systems are investigated. On the other hand, simple—and sometimes *too* simple—model calculations are performed in order to explain experimental results, thereby neglecting occasionally important aspects of the system under consideration. Apparently, there is a considerably large gap to be filled between the advanced electronic-structure and the model calculations.

The giant magneto-resistance (GMR) had and still has a huge impact on industrial applications [3]. The tunnel magneto-resistance (TMR), however, is expected to have even more potential for future applications and devices [4, 5]. From a theoretical point of view, TMR has the advantage that it can be understood in terms of simple quantum-mechanical effects (e.g., the tunnel effect) and can be modeled rather easily. Therefore, it lends itself support for an investigation which connects model calculations to the frontiers of nanoscience.

The purpose of the present paper is to provide a theory of spin-dependent transport through tunnel junctions which bridges the aforementioned gap. Its framework is the Landauer-Büttiker theory [6], in which elastic and ballistic transport is viewed as transmission of scattering channels through the device. All ingredients needed for the calculations of the tunnel conductance can be computed step-by-step, therefore allowing for simplifications or extensions. The theory outlined here was implemented one-to-one in a set of MATHEMATICATM notebooks [7], in order to obtain numerical results. Hence, the properties of the tunnel junction can be easily manipulated, results for different set-ups computed and visualized rapidly [8].

Model calculations typically assume free electrons in the metallic leads that are connected to the tunnel barrier, whereas electronic-structure calculations deal with a much more complicated bandstructure. An important feature of the latter—which is missing in the former—are band gaps, i.e., energetic regions in which electronic states are not present. Obviously, these have a significant impact on the electronic transport. In order to take band gaps into account, we go beyond the free-electron approximation by applying the nearly-free-electron (NFE) model. Assuming one-dimensional leads, the theory is kept simple enough to be tractable semi-analytically but it contains already the relevant aspects of the electronic structure. Both ferromagnetic and nonmagnetic leads are discussed, because the results for the latter can easily be transferred to the magnetic case. We note in passing that tunnel junctions with ferromagnetic leads typically comprise transition metals (Fe, Co, Ni), the electronic structure of which cannot be described well within the free-electron model.

The paper is organized as follows. First, basic theories for ballistic transport which are

relevant to the current work are sketched (section 2). Having introduced the model for the tunnel junction (section 3), the electronic-structure calculations (section 4) and the treatment of tunneling (section 5) are presented. Representative results of the tunneling calculations are discussed in subsection 6.2, focusing first on tunnel junctions with nonmagnetic leads (subsection 6.1). Spin-dependent transport is investigated in subsection 6.2.

2. Basic theories for ballistic transport

The theory presented in the forthcoming sections applies to elastic and ballistic transport of electrons through a tunnel junction (figure 1). Hence, the method of wavefunction matching for calculating the scattering wavefunction in the entire tunnel junction can be applied. Experimentally, ballistic transport is observed for small and defect-free samples.

The simplest approach to tunnel magneto-resistance traces back to the work of Jullière [9], where TMR is related to the polarization of the junction defined via spin-dependent *numbers of states* at the Fermi energies E_F in the leads. Maekawa and Gafvert [10] modified this model by defining the polarization in terms of the *densities of states* at E_F .

In the Landauer-Büttiker theory [11], the conductance is proportional to the transmission probability of the scattering channels (“conductance by transmission”), $G \propto T(E_F)$. For a tunnel junction, the scattering channels are the eigenstates of the leads in absence of the tunnel barrier, i. e., the Bloch states. This approach can be applied in both sophisticated electronic-structure calculations or in model calculations. For example, Slonczewski assumed free electrons in the ferromagnetic leads and a step-shaped tunnel barrier (as sketched in figure 1) [12].

The present work goes beyond Slonczewski’s model, in that it takes into account the nonzero potential in the leads. Applying the NFE model, the occurrence of band gaps in the electronic structure has a profound effect on the electronic transport. For the tunnel barrier, we stick with the step shape, being aware that a differently shaped barrier will lead to quantitatively different conductances [13]. The qualitative picture, however, will still be valid [14]. Although being computed in the framework of the Landauer-Büttiker theory, the present results can also be interpreted in terms of the densities of states.

3. Model for the tunnel junction

The one-dimensional tunnel junction consists of three regions: the left lead $\mathcal{L} = \{x|x < -d/2\}$, the barrier $\mathcal{B} = \{x|-d/2 \leq x \leq d/2\}$, and the right lead $\mathcal{R} = \{x|d/2 < x\}$. To keep the model as simple as possible, the leads were chosen identical, i. e., identical lattice spacing and potential (This restriction can, however, be relaxed in the MATHEMATICATM notebooks [8]). Within the leads, atoms are positioned at $x = -(d/2 + na)$ and $x = +(d/2 + na)$ for \mathcal{L} and \mathcal{R} , respectively (with n semi-positive integer). The lattice spacing a serves as the unit of length.

In accordance with the above spatial decomposition, the potential of the tunnel junction consists also of three parts (figure 2), namely $V^{\mathcal{L}}$, $V^{\mathcal{B}}$, and $V^{\mathcal{R}}$. The barrier potential $V^{\mathcal{B}}(x)$

is assumed constant, with value $V_{\text{barr}} > 0$. In principle, any other shape could be used [15]. In the leads, the potential is periodic, i. e., $V^{\mathcal{L}}(x) = V^{\mathcal{L}}(x - a)$ and $V^{\mathcal{R}}(x) = V^{\mathcal{R}}(x + a)$.

4. Calculation of the electronic structures

4.1 Electronic structure of the leads

According to the Landauer-Büttiker theory, one needs to compute the scattering channels, i. e., the electronic states of the leads in absence of the tunnel barrier. Thus, the lead potential extends over the whole x -axis.

The Schrödinger equation $H\psi = E\psi$ in atomic units [16] reads

$$\left[\frac{1}{2} \frac{d^2}{dx^2} + V(x) \right] \psi(x) = E\psi(x). \quad (1)$$

Expanding the periodic potential into a Fourier series,

$$V(x) = \sum_{q \in \mathbb{Q}} V_q e^{iqx}, \quad (2)$$

the requirement of periodicity [$V(x) = V(x + na)$, n integer] restricts q immediately to the reciprocal lattice \mathbb{Q} , i. e., $q \in \mathbb{Q} = \{ng | n \text{ integer}, g = 2\pi/a\}$. The mean value V_0 of the potential serves as origin of the energy scale and, hence, is set to zero ($V_0 = 0$). Assuming further a real $V(x)$ and the mirror symmetry $V(x) = V(-x)$, one has $V_{-q} = V_q \forall q \in \mathbb{Q}$. For free electrons, $V(x)$ vanishes identically ($V_q = 0 \forall q \in \mathbb{Q}$).

For a periodic potential, the eigenstates ψ of the Hamiltonian H fulfill Floquet's theorem [17]. In analogy to (equation 2), the Bloch states are as well expanded into a Fourier series,

$$\psi_k(x) = e^{ikx} \sum_{q \in \mathbb{Q}} c_q(k) e^{iqx}. \quad (3)$$

In the following, the Schrödinger equation is solved by two methods, which have in common that the differential equation is transformed into an algebraic set.

4.1.1 Computation of $E(k)$. Inserting equation (2) and equation (3) into the Schrödinger equation (1) gives the infinite algebraic set

$$\left[\frac{1}{2} (q + k)^2 \right] c_q(k) + \sum_{q' \in \mathbb{Q}} V_{q-q'} c_{q'}(k) = E(k) c_q(k), \quad \forall q \in \mathbb{Q}, \quad (4)$$

with $k \in] -g/2, g/2[$. Defining

$$H_{qq'}(k) = \frac{1}{2} (q + k)^2 \delta_{qq'} + V_{q-q'}, \quad \forall q, q' \in \mathbb{Q}, \quad (5)$$

one obtains the compact form

$$\sum_{q' \in \mathbb{Q}} H_{qq'}(k) c_{q'}(k) = E(k) c_q(k), \quad \forall q \in \mathbb{Q}, \quad (6)$$

which can be cast into matrix form, $H(k)\mathbf{c}(k) = E(k)\mathbf{c}(k)$. The Hamilton matrix $H(k)$ is square and hermitian, resulting in real eigenvalues $E(k)$.

4.1.2 Computation of $k(E)$. In tunneling calculations, an electron is specified by its energy E . Since the Bloch states in each lead are characterized by the wavenumber $k^{\mathcal{L}}$ and $k^{\mathcal{R}}$, respectively, it has to be assured that $E(k^{\mathcal{L}}) = E(k^{\mathcal{R}}) = E$. Alternatively, one could solve for $k(E)$ in each lead, an obviously favorable method [18].

Rewriting equation (4) as

$$\left(q - \sqrt{2(E + V_0)} + k \right) \left(q + \sqrt{2(E + V_0)} + k \right) c_q + 2 \sum_{q' \in \mathbb{Q} \setminus q} V_{q-q'} c_{q'} = 0, \quad \forall q \in \mathbb{Q}, \quad (7)$$

an algebraic set of double rank as in the $E(k)$ approach is obtained by defining auxiliary expansion coefficients w_q :

$$\begin{aligned} (q - \sqrt{2(E + V_0)} + k) w_q + 2 \sum_{q' \in \mathbb{Q} \setminus q} V_{q-q'} c_{q'} &= 0, \\ -w_q + (q + \sqrt{2(E + V_0)} + k) c_q &= 0. \end{aligned} \quad (8)$$

In matrix form, equation (8) reads

$$\begin{pmatrix} h_{11}(E) & h_{12}(E) \\ h_{21}(E) & h_{22}(E) \end{pmatrix} \begin{pmatrix} \mathbf{w}(E) \\ \mathbf{c}(E) \end{pmatrix} = k(E) \begin{pmatrix} \mathbf{w}(E) \\ \mathbf{c}(E) \end{pmatrix}, \quad (9)$$

where the Hamilton matrix $H(E)$ is a 2×2 supermatrix comprising submatrices h_{ij} of rank $r_{\mathbb{Q}}$,

$$\begin{aligned} h_{qq'}^{(11)} &= (q - \sqrt{2(E + V_0)}) \delta_{qq'}, & \forall q, q' \in \mathbb{Q}, \\ h_{qq'}^{(22)} &= (q + \sqrt{2(E + V_0)}) \delta_{qq'}, \\ h_{qq'}^{(12)} &= 2 V_{|q-q'|} (1 - \delta_{qq'}), \\ h_{qq'}^{(21)} &= -\delta_{qq'}. \end{aligned} \quad (10)$$

Since $H(E)$ is not hermitian, its $2r_{\mathbb{Q}}$ eigenvalues $k^{(i)}(E)$ can be complex. The dispersion relation $k(E)$ defines then the complex band structure [19]. For the tunneling, real $k^{(i)}$ are appropriate because only these belong to square-integrable wavefunctions [$\psi^{(i)} \in L_2(-\infty, +\infty)$ for $k^{(i)}$ real]. If, however, $\text{Im } k^{(i)} > 0$ ($\text{Im } k^{(i)} < 0$), the eigenfunction $\psi^{(i)}$ decays exponentially towards $+x$ ($-x$) [20].

5. Calculation of tunneling

Having specified the electronic states in the three regions \mathcal{L} , \mathcal{B} , and \mathcal{R} , the wavefunction in the entire tunnel junction at a given energy E has to be determined. This is achieved by requiring continuity of the total wavefunction and of its first spatial derivative at the two interfaces \mathcal{L} - \mathcal{B} at $x = -d/2$ and \mathcal{B} - \mathcal{R} at $x = d/2$ (figure 2).

While the Schrödinger equation determines the functional form of the wavefunctions in the three regions, their actual shape has to be determined by the boundary conditions. Since tunneling is viewed as scattering of an incoming electron at the barrier (figure 1), scattering boundary conditions have to be applied. Note that only electrons in occupied states of the source electrode can tunnel into unoccupied states of the drain electrode, due to the Pauli exclusion principle.

Assume for the following that the wavefunctions in the leads and in the barrier at energy E have been computed according to the approaches introduced in section 4. Since E is fixed, the explicit energy dependence will be dropped.

5.1 Nonmagnetic leads

5.1.1 Determination of the total wavefunction. In the present one-dimensional model, there is only a single Bloch state in each lead with positive (or negative) velocity. Thus, the total wavefunction in \mathcal{L} is superposed by the incoming Bloch state $\psi_i(x)$ (with velocity $v_i > 0$) and the reflected Bloch state $r\psi_r(x)$ (with velocity $v_r = -v_i$), $\psi_i(x) + r\psi_r(x)$. In \mathcal{R} there is only the transmitted Bloch state $t\psi_t(x)$ with $v_t > 0$ (figure 1). Within the barrier \mathcal{B} , two exponential functions are taken, $A \exp(\kappa x) + B \exp(-\kappa x)$. The matching conditions provide the probabilities for transmission through and reflection at the barrier given by $|t|^2$ and $|r|^2$, respectively.

Within Landauer-Büttiker theory, reservoirs contribute each incoming scattering channel with the same current j_i . Therefore, either the Bloch states [12] or the transmission probabilities have to be normalized to unit current,

$$T = |t|^2 \frac{j_t}{j_i}, \quad (11)$$

with the current j_t carried by ψ_t being calculated from $j = \text{Im}(\psi^* \frac{d}{dx} \psi)$. The transmission T measures the transmitted current which is carried by ψ_t upon feeding with ψ_i . Current conservation implies $(1 - |r|^2)j_i = |t|^2 j_t$.

5.1.2 Current and conductance. Applying a bias voltage V_{bias} to the tunnel junction shifts the Fermi energies of the electrodes, as is shown schematically in figure 3. For zero bias, the Fermi energies E_F of the electrodes \mathcal{L} and \mathcal{R} coincide ($E_F^{\mathcal{L}} = E_F^{\mathcal{R}}$, figure 3a). For $V_{\text{bias}} > 0$, the potential $V^{\mathcal{R}}(x)$ is shifted rigidly to lower energies, which is achieved by taking as potential average $V_0 = -V_{\text{bias}}$ instead of $V_0 = 0$ (as being fixed for \mathcal{L}). Evidently, both the band structure and the Fermi energy of \mathcal{R} are shifted alike, $E^{\mathcal{R}}(k) = E^{\mathcal{L}}(k) - V_{\text{bias}}$ and $E_F^{\mathcal{R}} = E_F^{\mathcal{L}} - V_{\text{bias}}$ (figure 3b). Hence, electrons can tunnel from \mathcal{L} to \mathcal{R} . Since

only electrons of occupied states in \mathcal{L} (with energy $E < E_F^{\mathcal{L}}$) can tunnel into unoccupied electronic states in \mathcal{R} ($E_F^{\mathcal{L}} - V_{\text{bias}} < E$), an energy window opens up in which tunneling can take place ($E \in [E_F^{\mathcal{L}} - V_{\text{bias}}, E_F^{\mathcal{L}}]$, cf. the orange areas in figure 3).

The total current I through the tunnel junction, which flows from the source electrode \mathcal{L} to the drain electrode \mathcal{R} , can be expressed for small V_{bias} (linear response) as $I = G V_{\text{bias}}$. Within Landauer-Büttiker theory, it is given by the sum over all transmission probabilities $T(E)$ in the energy window $[E_F^{\mathcal{L}} - V_{\text{bias}}, E_F^{\mathcal{L}}]$,

$$I = G_0 \int_{E_F^{\mathcal{L}} - V_{\text{bias}}}^{E_F^{\mathcal{L}}} T(E) dE. \quad (12)$$

In general, $T(E)$ implies a sum over the transmission probabilities of all incident Bloch states ψ_i and all transmitted Bloch states ψ_t . In the present one-dimensional model, with a single electronic state available in each electrode, $T(E)$ reduces to a single term [cf equation (11)]. The quantum of conductance G_0 is 4π in atomic units ($2e^2/h$), where the factor 2 comes from the spin degeneracy. In experiments, the differential conductance dI/dV_{bias} is typically recorded, which is computed numerically from equation (12).

The conductance G of the tunnel junction,

$$G = \frac{G_0}{V_{\text{bias}}} \int_{E_F^{\mathcal{L}} - V_{\text{bias}}}^{E_F^{\mathcal{L}}} T(E) dE, \quad (13)$$

depends on details of the tunnel junction via the transmission $T(E)$, e. g., on the electrode band structures and properties of the tunnel barrier.

5.2 Ferromagnetic leads

In nonmagnetic systems, each electronic state can be occupied by two electrons, one with spin up, the other with spin down. The spin-dependent band structures of each lead coincide [$E_{\pm}^{\mathcal{L}}(k) = E(k)$ and $E_{\pm}^{\mathcal{R}}(k) = E(k) - V_{\text{bias}}$] and the number of spin-up electrons equals the number of spin-down electrons. This degeneracy is lifted in magnetic systems, and the spin-dependent band structures are rigidly shifted by the exchange splitting $V_{\text{ex}} > 0$ with respect to each other, i. e., $E_{\pm}^{\mathcal{L}}(k) = E(k) \mp V_{\text{ex}}/2$ and $E_{\pm}^{\mathcal{R}}(k) = E(k) - V_{\text{bias}} \mp V_{\text{ex}}/2$ (4). Since the electronic states are occupied up to the Fermi energy E_F , there are usually more spin-up electrons than spin-down electrons, which leads to the notation majority (minority) electrons indicated by “+” (“−”).

Associating majority (minority) with spin-up (spin-down) electrons in \mathcal{L} [21], defines a net magnetic moment $\mathbf{M}^{\mathcal{L}}$ which is parallel to the magnetic moments of the electrons, due to the surplus of majority electrons. In a magnetic tunnel junction two configurations remain for the right lead. Either the net magnetic moment $\mathbf{M}^{\mathcal{R}}$ in \mathcal{R} is parallel to that in \mathcal{L} ($\mathbf{M}^{\mathcal{L}} \parallel \mathbf{M}^{\mathcal{R}}$) which is called P configuration or anti-parallel ($\mathbf{M}^{\mathcal{L}} \parallel -\mathbf{M}^{\mathcal{R}}$) which is called AP configuration, respectively.

In experiment, the configurations can be switched by an external mag Because the spin is conserved during the tunneling process, the total current in each configuration is given

by the sum of the two spin-resolved currents (“two current model”). In P configuration, with electrons tunneling from majority (minority) states into majority (minority) states, one has the upper situation of figure 5

$$I_P = I_{++} + I_{--}, \quad (14)$$

and accordingly for the AP configuration, with majority and minority interchanged in \mathcal{R} (bottom in figure 5),

$$I_{AP} = I_{+-} + I_{-+}. \quad (15)$$

The four spin-dependent currents are related to the conductance contributions $G_P = G_{++} + G_{--}$ and $G_{AP} = G_{+-} + G_{-+}$. The quantum of conductance G_0 is now 2π (i.e., e^2/h). For a nonmagnetic junction, all spin-resolved currents are identical ($I_{++} = I_{--} = I_{-+} = I_{+-}$).

In typical tunnel junctions in P configuration, one of the spin-resolved currents exceeds the other by far (for instance, $I_{++} \gg I_{--}$ in figure 5), whereas in AP configuration, both currents are of almost the same size ($I_{+-} \approx I_{-+}$). The tunnel magneto-resistance (TMR) δ is a measure for the spin-dependent transport and defined here by the asymmetry of I_P and I_{AP} ,

$$\delta = \frac{I_P - I_{AP}}{I_P + I_{AP}} = \frac{G_P - G_{AP}}{G_P + G_{AP}}. \quad (16)$$

The tunneling calculations for ferromagnetic leads proceed as those for nonmagnetic leads but with the band structures shifted by $\mp V_{\text{ex}}/2$, giving rise to the four currents $I_{\pm\pm}$. Eventually, I_P , I_{AP} , and δ are computed from the latter.

6. Results and discussion

The theory of tunneling, as described in the preceding sections, was implemented in a set of MATHEMATICATM notebooks [8]. Because the results for a magnetic tunnel junction (subsection 6.2) can easily be understood from those for a nonmagnetic one, the latter are presented and discussed first. For the following, the basis set is $\mathbb{Q} = \{-3g, -2g, \dots, +2g\}$ ($r_{\mathbb{Q}} = 6$). The Fourier coefficients V_q of the lead potentials are chosen as $V_0 = 0$ H, $V_g = 0.012$ H, $V_{2g} = 0.008$ H, and $V_{3g} = 0.004$ H.

6.1 Nonmagnetic leads

6.1.1 Nearly-free *vs* free electrons. The Hamilton matrix for free electrons is diagonal ($V_q = 0$), and the Bloch states become pure plane waves, $\phi^{(q)} = \exp[i(k + q)x]$, with band structure $E^{(q)}(k) = (k + q)^2/2$ and velocities $v^{(q)}(k) = k + q$. The density of states decreases with energy, $D(E) = 2\pi dk(E)/dE = \pi\sqrt{2/E}$.

The nonzero potential in the NFE case results in band gaps at $k = 0$ and $k = \pm g/2$. The band gaps at $k = \pm g/2$ are between band 1 (lowest in energy, black in figure 6a and 6e) and band 2 (orange) and show up between 0.112 H and 0.137 H. The first gap at $k = 0$ appears at 0.492 H between bands 2 and 3. The band widths are much larger than the band gaps. For band 1, for instance, the band width is $E^{(1)}(g/2) - E^{(1)}(0) = 0.112 \text{ H} + 0.006 \text{ H} = 0.118 \text{ H}$,

whereas the band gap is $E^{(2)}(g/2) - E^{(1)}(g/2) = 0.025H$. Thus, the electrons behave as *nearly free* (NF), that is, the electronic properties differ from those of free electrons in the small energy ranges at the band gaps.

The velocities $v^{(i)}(k) = dE^{(i)}(k)/dk$ for NF electrons (figure 6b) which are linear in a large part of the BZ, vanish at the band edges ($k = \pm g/2$ and $k = 0$). Further, they change sign at $k = 0$. Since electrons with zero velocity cannot contribute to the current, a considerable effect on the tunnel current is expected at the band gaps. The DOS $D(E)$ (figure 6e) also resembles that of free electrons but becomes singular at the band edges. These Van-Hove singularities will also show up in the tunnel current. Considering the NFE Bloch states, the expansion coefficient $c_0^{(1)}$ of band 1 dominates in a large part of the BZ, that is, the wavefunction is to a very good approximation equal to the single plane wave with $q = 0$ (figure 6c). At $k = \pm g/2$, other plane waves become mixed in: $|c_{-g}^{(1)}| > 0$ at $k = +g/2$ and $|c_g^{(1)}| > 0$ at $k = -g/2$. Band 2 shows the same qualitative behaviour, but in addition mixing at $k = 0$. In summary, differences between free and nearly-free electrons in the leads show up close to band gaps.

In order to work out how the tunneling is modified with respect to that of free electrons, the transmissions $T(E)$ vs barrier width d are compared for energies close to and well below the band gap at $k = g/2$. For $d = 0$, the transmission is perfect in all cases [$T(E) = 1$] because the incoming Bloch states are not reflected at the barrier (figure 7a). With increasing d , $T(E)$ decreases due to the decaying wavefunctions in \mathcal{B} . For $E = 0.112H$, i. e., close to the band edge, the transmission for free electrons is significantly larger than for NF electrons, as can be explained by their larger velocity. On the contrary, there is no apparent difference for E well below the band edge (here: $E = 0.050H$) because in both cases the Bloch states comprise a single plane wave. In summary, band gaps have a pronounced effect on the transmission and show also up in the bias dependence of the current.

6.1.2 Bias dependence of tunneling. Before turning to current and conductance, the dependence of the transmission on bias voltage and barrier width is addressed for fixed energy (figure 7b). The overall smooth shape is disturbed by sharp minima at about $0.013H$ and $0.4H$ bias which are related to the band gaps in \mathcal{R} . The monotonous decay with barrier width d is consistent with that in figure 7.

At first glance, one would expect that a current I through a tunnel junction increases with bias voltage, in accordance with Ohm's law. This behaviour can indeed be observed in figure 8a, but only as a general trend. For bias below $0.1H$ and at about $0.4H$ ample deviations occur, with I showing even a decrease. These features show up more pronounced in the differential conductance dI/dV (figure 8b), where the linear dependence of I on bias can be clearly resolved between $0.10H$ and $0.35H$. The conductance drops rapidly with bias but remains almost constant for $V_{\text{bias}} > 0.1H$ (figure 8c).

The aforementioned features can be discussed in terms of band structures and transmission probabilities. However, a simpler access is provided by the number of states within the energy window of tunneling $[E_F^{\mathcal{L}} - V_{\text{bias}}, E_F^{\mathcal{L}}]$, an approach to be viewed as an extension of

the Maekawa-Gafvert model to nonzero bias (section 2). The number $N_i^{\mathcal{L}}(V_{\text{bias}})$ of incident states in \mathcal{L} is

$$N_i^{\mathcal{L}}(V_{\text{bias}}) = \frac{1}{2} \int_{E_{\text{F}}^{\mathcal{L}} - V_{\text{bias}}}^{E_{\text{F}}^{\mathcal{L}}} D^{\mathcal{L}}(E) dE, \quad (17)$$

where the factor $1/2$ takes into account that only half of the Bloch states show positive velocity. For $E_{\text{F}}^{\mathcal{L}}$ within band 1 (at 0.1 H), $N_i^{\mathcal{L}}$ increases monotonously until $V_{\text{bias}} = E_{\text{F}}^{\mathcal{L}} - E_{\text{bot}}^{\mathcal{L}}$, i.e., when the bottom of band 1 is reached [$E_{\text{bot}}^{\mathcal{L}} = E^{(1)}(0)$; figure 8d]. Because $N_i^{\mathcal{L}}$ remains constant for larger bias (figure 3 and figure 6), it is sufficient to restrict the integration in equation (17) to $[E_{\text{min}}^{\mathcal{L}}, E_{\text{F}}^{\mathcal{L}}]$, with $E_{\text{min}}^{\mathcal{L}} = \max(E_{\text{bot}}^{\mathcal{L}}, E_{\text{F}}^{\mathcal{L}} - V_{\text{bias}})$.

The number $N_t^{\mathcal{R}}(V_{\text{bias}})$ of transmitted states in \mathcal{R} depends on the energy range in which incident electrons are provided by \mathcal{L} . Thus,

$$N_t^{\mathcal{R}}(V_{\text{bias}}) = \frac{1}{2} \int_{E_{\text{min}}^{\mathcal{L}}}^{E_{\text{F}}^{\mathcal{L}}} D^{\mathcal{R}}(E) dE. \quad (18)$$

As is evident from figure 8d, the general shape of $N_t^{\mathcal{R}}$ consists of an increase for bias up to about 0.13 H and a slight decrease for larger bias. But on top of this, it shows a richer structure than $N_i^{\mathcal{L}}$. Upon increasing V_{bias} , a kink appears either when a band edge enters the energy windows (at $E_{\text{F}}^{\mathcal{L}}$) or when it leaves the window (at $E_{\text{min}}^{\mathcal{L}}$). This is supported by considering the DOS of \mathcal{R} at the boundaries of the energy window from (figure 8e). At the upper boundary [$D^{\mathcal{R}}(E_{\text{F}}^{\mathcal{L}})$, black in figure 8e], a band gap produces a decrease of the current since there are less transmitted states available. The lower boundary [$D^{\mathcal{R}}(E_{\text{min}}^{\mathcal{L}})$, orange], however, shows much less effect. The small kink in I and G at 0.1 H is due to $N_i^{\mathcal{L}}$, because it appears just when $E_{\text{F}}^{\mathcal{L}} - E_{\text{bot}}^{\mathcal{L}} = V_{\text{bias}}$.

In summary, the structures in the bias dependence of both the current and the conductance can be explained by the density of states at the boundaries of the tunnel-energy window and by the number of incoming and transmitted states. The actual current, however, is further influenced by the tunneling probability which appears to be of minor importance due to its smooth shape.

6.2 Ferromagnetic leads

Having investigated the transport properties of tunnel junctions with nonmagnetic leads, we now turn to junctions with ferromagnetic leads. With regard to subsection 5.2, the spin-dependent currents $I_{\pm\pm}$ and conductances $G_{\pm\pm}$ were obtained from calculations for nonmagnetic leads in which the band structures $E_{\pm}(k)$ were rigidly shifted by the exchange splitting $\mp V_{\text{ex}}/2$ (chosen as 0.03 H in the following).

Considering the conductances for the P configuration (figure 9a), the arbitrarily chosen exchange splitting V_{ex} causes a bias dependence of the conductance contribution G_{--} which is very similar to the nonmagnetic case (figure 8b). The conductance contribution G_{++} , however, is zero for small bias until the bias bridges the gap to the top of band 1 in \mathcal{L} . For larger bias, G_{++} is finite but always much smaller than G_{--} . Consequently, G_{P} is mainly determined by G_{--} (figure 9a).

In comparison to the P configuration, the conductances in AP configuration appear slightly modified. G_{-+} is zero until V_{bias} bridges the gap to the bottom of band 2 in \mathcal{R} . It increases until a maximum is reached, drops rapidly, and remains almost constant for $V_{\text{bias}} > 0.1 \text{ H}$ until the next gap occurs. $G_{-+}(\text{AP})$ is similar to $G_{--}(\text{P})$ but the corresponding extrema are shifted to lower energies by V_{ex} . $G_{+-}(\text{AP})$ is similar to $G_{++}(\text{P})$ with the same onset at bias voltages reaching the top of band 1 in \mathcal{L} . G_{AP} is determined by G_{-+} .

The tunnel magneto-resistance δ (equation 16) shows a pronounced bias dependence which is related to the bandstructure, especially to the position of the bandgaps of the leads (figure 9c). First of all, a zero-bias anomaly shows up which is caused by the half-metallic behaviour of the leads. This is—in contrast to other explanations [22]—a pure electronic effect. In general, δ decays with increasing V_{bias} except the influence at the bandgaps. As discussed above (figure 8), a bandgap in \mathcal{R} at the upper boundary of the energy window causes a decrease of the conductance. Minima in G_{P} manifest themselves as minima in δ . Conductance minima at G_{AP} (G_{-+}) cause maxima at $V_{\text{bias}} = 0.036 \text{ H}$ and 0.39 H . These maxima and the subsequent minima are separated by V_{ex} .

Concerning the thickness dependence of the tunneling magneto-resistance: the absolute values of δ increase. Hence, the characteristic features of δ become more pronounced. The reason for this behavior is related to the fact that $G_{\text{P}} + G_{\text{AP}}$ drops faster with increasing barrier thickness than $G_{\text{P}} - G_{\text{AP}}$.

7. Concluding remarks

The main purpose of this paper was to demonstrate the role of a realistic bandstructure of the leads, described within a NFE model, for the current-voltage characteristics of tunnel junctions. The consideration was extended to ferromagnetic junctions in order to discuss the bias dependence of the tunnel magneto-resistance. In difference to a free-electron model a pronounced TMR effect was obtained. The TMR reveals a zero-bias anomaly of electronic origin caused by the half-metallic behaviour of the leads. Driven by the position of the band gaps in the drain electrode, with respect to the Fermi energy in the source electrode, pronounced positive and negative TMR values occur.

As further extensions to the presented theory, one could conceive to discuss the spin polarizations defined in terms of the number of electrons in the leads and of the spin-resolved currents $I_{\pm\pm}$. Contact to the popular Jullière and the Maekawa-Gafvert models [9, 10] can be made by trying to explain the TMR δ by these spin polarizations. However, one has to be aware that a possible agreement does not hold in general for three-dimensional models because in one dimension the conductance is related simply to the number of states in the leads. Another issue could involve different leads which result in a nonsymmetric current-voltage characteristics [$I(V_{\text{bias}}) \neq -I(-V_{\text{bias}})$].

References

- [1] S. Maekawa, T. Shinjo (Editors), *Spin Dependent Transport in Magnetic Nanostructures* (Taylor & Francis, London, 2002).
- [2] I. Žutić, J. Fabian, S. Das Sarma, Rev. Mod. Phys. **76** 323 (2004).
- [3] J. M. Daughton, J. Magn. Magn. Mater. **192** 334 (1999).
- [4] D. Grundler, Physics World **15** 39 (2002).
- [5] T. J. Klemmer, J. Z. Sun, A. Fert, J. Bass (Editors), *Spintronics*, volume 260 of *Symposium Proceedings* (Materials Research Society, Warrendale, 2002).
- [6] Y. Imry, R. Landauer, Rev. Mod. Phys. **71** S306 (1999).
- [7] S. Wolfram, *The MATHEMATICA book* (Wolfram Media, Champaign, 1996), URL: <http://www.wolfram.com>.
- [8] The notebooks for MATHEMATICA version 5 can be obtained from the authors. Electronic addresses: bose@physik.uni-halle.de, mertig@physik.uni-halle.de, and henk@mpi-halle.de.
- [9] M. Jullière, Phys. Lett. A **54** 225 (1975).
- [10] S. Maekawa, U. Gafvert, IEEE Transact. Magn. **MAG-18** 707 (1982).
- [11] M. Büttiker, Y. Imri, R. Landauer, S. Pinhas, Phys. Rev. B **31** 6207 (1985).
- [12] J. C. Slonczewski, Phys. Rev. B **39** 6995 (1989).
- [13] I. I. Mazin, Europhys. Lett. **55** 404 (2001).
- [14] O. M. Probst, Am. J. Phys. **70** 1110 (2002).
- [15] Y. Ando, T. Itoh, J. Appl. Phys. **61** 1497 (1987).
- [16] Atomic Hartree units are used, $e = \hbar = m = 1$, $c \approx 137.036$. $1 \text{ H} \approx 27.12 \text{ eV}$.
- [17] A. A. Cottey, Am. J. Phys. **39** 1235 (1971).
- [18] J. B. Pendry, J. Phys. C: Sol. State Phys. **2** 2273 (1969).
- [19] V. Heine, Proc. Phys. Soc. **81** 300 (1963).
- [20] J. C. Slater, Phys. Rev. **51** 840 (1937).
- [21] B. T. Jonker, A. T. Hanbicki, D. T. Pierce, M. D. Stiles, J. Magn. Magn. Mater. **277** 24 (2004).
- [22] S. Zhang, P. M. Levy, A. C. Marley, S. S. P. Parkin, Phys. Rev. Lett. **79** 3744 (1997).

Figure captions

Figure 1: Sketch of a tunnel junction with ferromagnetic leads (\mathcal{L} , \mathcal{R}) and a step-shaped barrier (\mathcal{B}). An electron incident from the left (with current j_i) is reflected (current j_r) and transmitted through \mathcal{B} into \mathcal{R} (j_t). In the leads, the potential depends on the spin of the electron: for a spin-up electron it is lower (\uparrow , dashed red line) than for a spin-down electron (\downarrow , solid red line).

Figure 2: Potential $V(x)$ of the tunnel junction. For the barrier \mathcal{B} , a step-shaped potential with height V_{barr} and width d is assumed. The potential in the leads \mathcal{L} and \mathcal{R} is periodic with the lattice spacing a . The interfaces between the three regions are at $x = \pm d/2$.

Figure 3: Sketches of the electronic structure of a tunnel junction with a bias voltage applied, as depicted schematically by the density of states (black areas) for the leads \mathcal{L} and \mathcal{R} . For zero bias, the Fermi energies E_F coincide (a), whereas for positive bias $E_F^{\mathcal{R}}$ is lowered to $E_F^{\mathcal{L}} - V_{\text{bias}}$ in \mathcal{R} , opening up the energy window of tunneling [orange area in (b–d)]. The size of the energy window increases with V_{bias} (b) until its lower boundary $E_F^{\mathcal{L}} - V_{\text{bias}}$ reaches the bottom $E_{\text{bot}}^{\mathcal{L}}$ of the \mathcal{L} -bands (c, d). The barrier is denoted \mathcal{B} .

Figure 4: Spin-resolved band structures in the ferromagnetic leads of a tunnel junction in P configuration. The majority-electron bands (+, black) are shifted by $V_{\text{ex}} > 0$ with respect to the minority bands (−, orange) in both leads. The junction is biased by $V_{\text{bias}} > 0$.

Figure 5: Configurations of a tunnel junction with ferromagnetic leads. The lead magnetizations are either parallel ($\mathbf{M}^{\mathcal{L}} \parallel \mathbf{M}^{\mathcal{R}}$; P configuration, top) or anti-parallel ($\mathbf{M}^{\mathcal{L}} \parallel -\mathbf{M}^{\mathcal{R}}$; AP configuration, bottom). The spin-resolved currents $I_{\pm\pm}$ are visualized by horizontal arrows.

Figure 6: Electronic structure of a nonmagnetic lead, with a focus either on the $E(k)$ (left: a–d) or on the $k(E)$ description (right: e–h). (a) Bandstructure $E(k)$ of the lowest (black, band 1) and the second (orange, band 2) band in the first Brillouin zone, $k \in]-g/2, g/2]$. (b) Velocity $v(k)$ of the corresponding Bloch states. (c, d) Fourier coefficients $c_q^{(i)}(k)$ of the Bloch states associated with band 1 (c) and 2 (d). (e) Bandstructure, but in $k(E)$ representation. (f) Density of states $D(E)$ for the bands shown in (a) and (d). (g, h) Fourier coefficients of (c) and (d), but for $k \geq 0$ (g) and $k \leq 0$ (h).

Figure 7: (a) Transmission T through an unbiased tunnel junction with nonmagnetic leads ($V_{\text{barr}} = 0.12 \text{ H}$). For energies close to ($E = 0.112 \text{ H}$; black lines) or well below ($E = 0.050 \text{ H}$; orange lines) the band gap at $k = g/2$ ($E = 0.112 \text{ H}$), $T(d)$ is plotted *vs* barrier width d for nearly-free (solid) and free (dotted) lead-electrons. (b) Transmission probability $T(E)$ *vs* bias and barrier width d at $E = 0.1 \text{ H}$.

Figure 8: Current-voltage characteristic of a tunnel junction with barrier width $d = 2.5a$ and nonmagnetic leads. (a–c) Total current I , differential conductance dI/dV_{bias} , and conductance G *vs* bias voltage. (d) Number of states incoming from \mathcal{L} (black) and outgoing in \mathcal{R} (orange). (e) Density of states of the right lead \mathcal{R} at $E_{\text{F}}^{\mathcal{L}}$ (black) and at $E_{\text{bot}}^{\mathcal{L}}$ (in units of the lattice constant). The Fermi energy is 0.1 H .

Figure 9: Spin-dependent tunneling for $E_{\text{F}} = 0.1 \text{ H}$ and exchange splitting $V_{\text{ex}} = 0.03 \text{ H}$. (a) Spin-dependent conductances G_{++} and G_{--} for the P configuration *vs* bias for barrier width $d = 2.5a$. Their sum is denoted G_{P} . (b) As for (a) but for the AP configuration, with $G_{\text{AP}} = G_{+-} + G_{-+}$. (c) Tunnel magneto-resistance δ obtained from the conductances of (a) and (b). (d) Dependence of the TMR δ on barrier width, as indicated by different line styles.

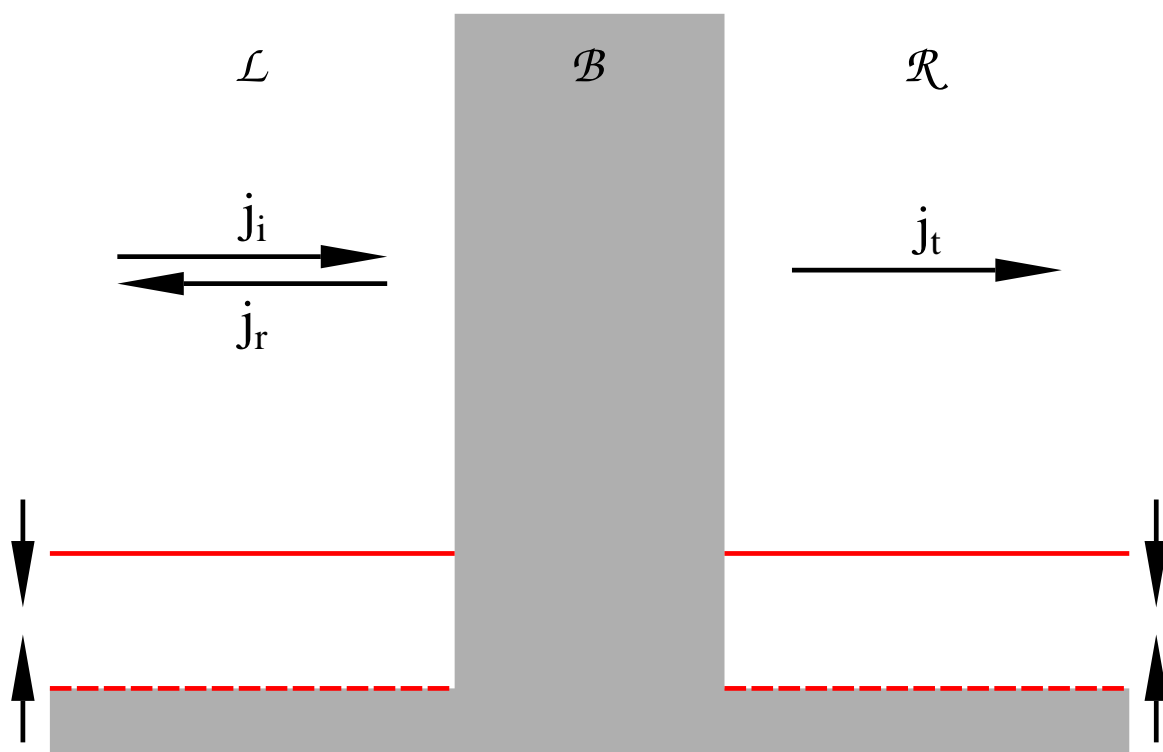


Figure 1

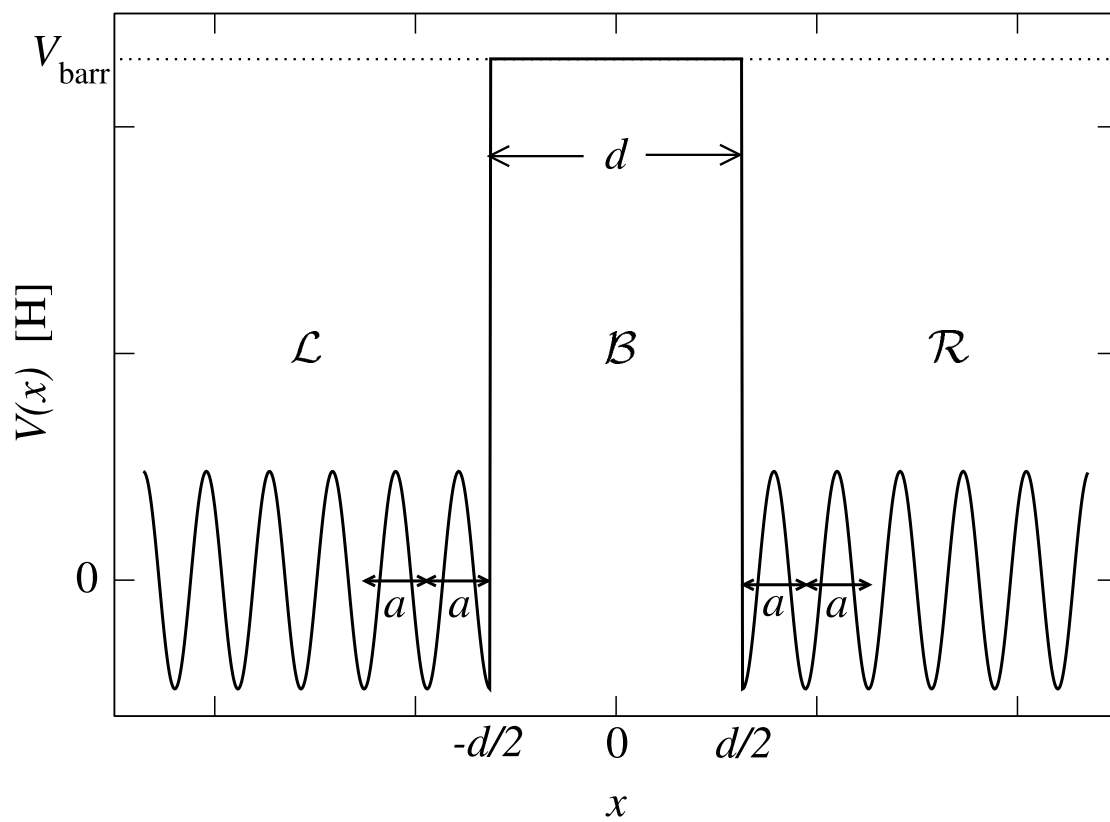


Figure 2

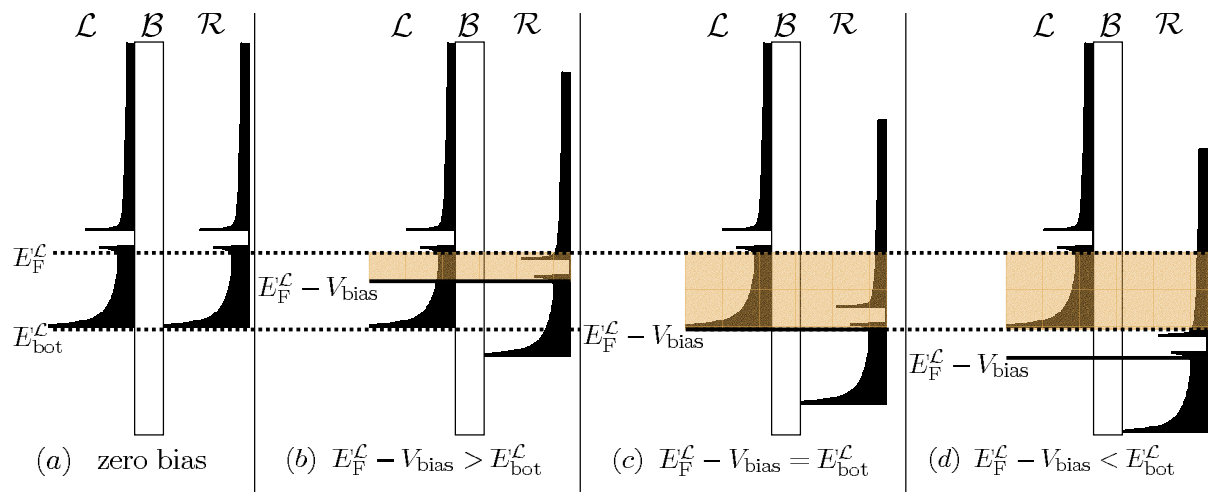


Figure 3

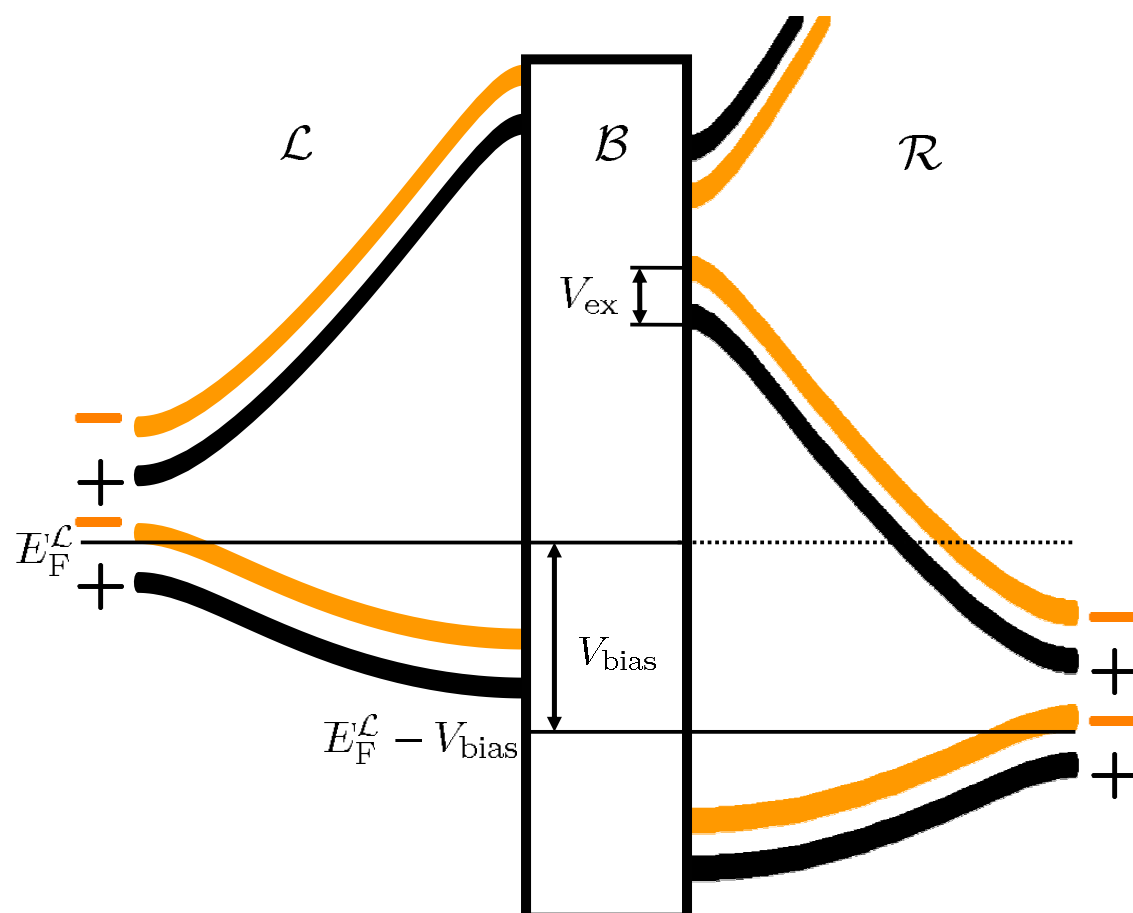


Figure 4

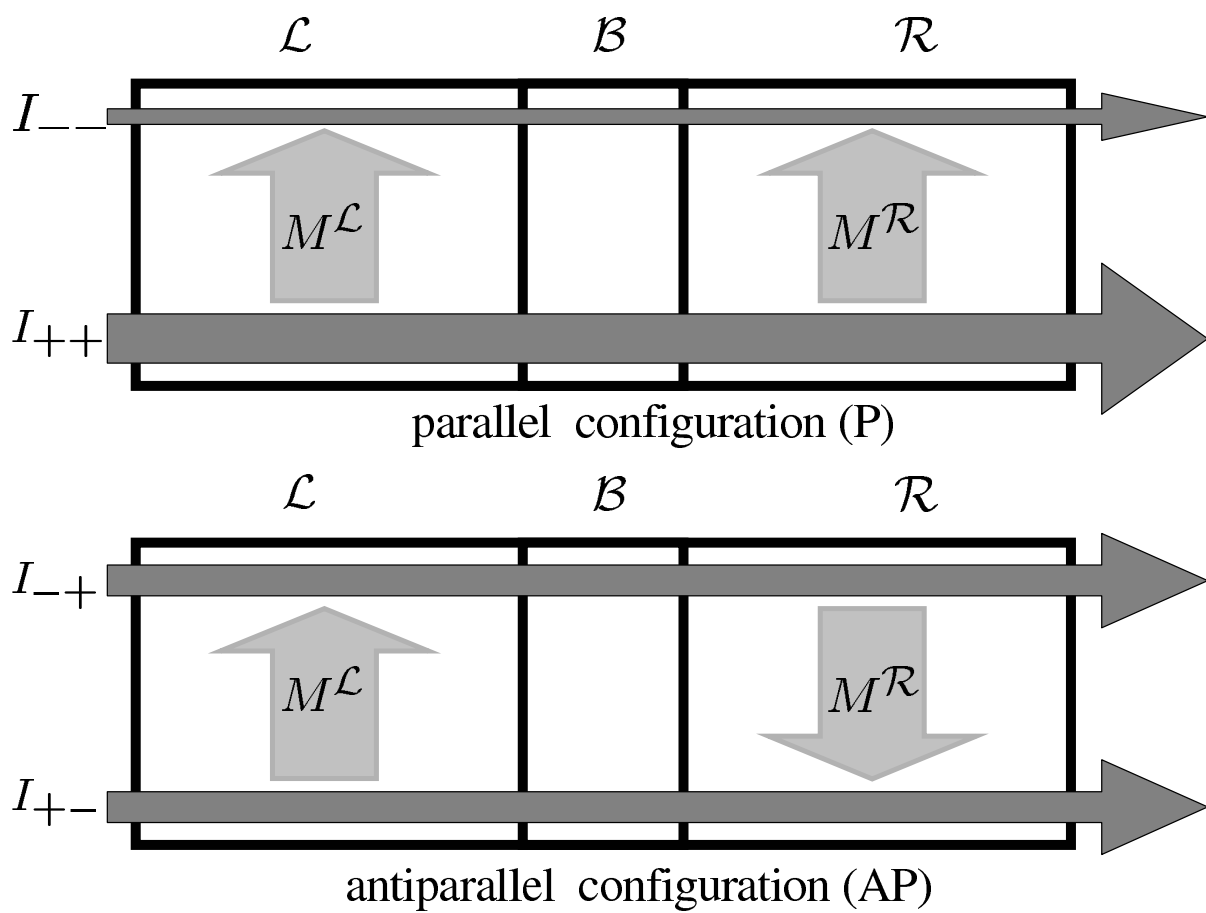


Figure 5

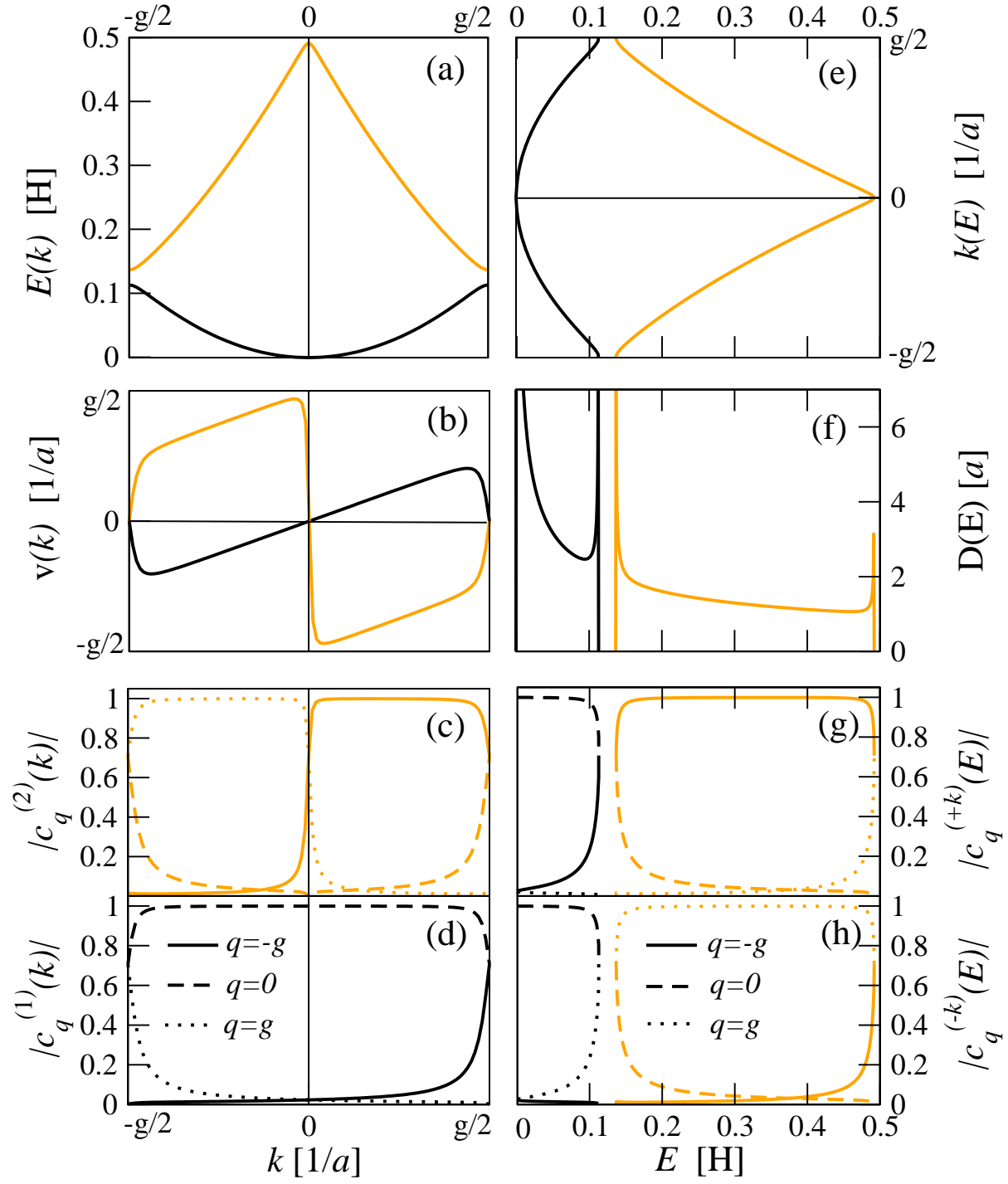


Figure 6

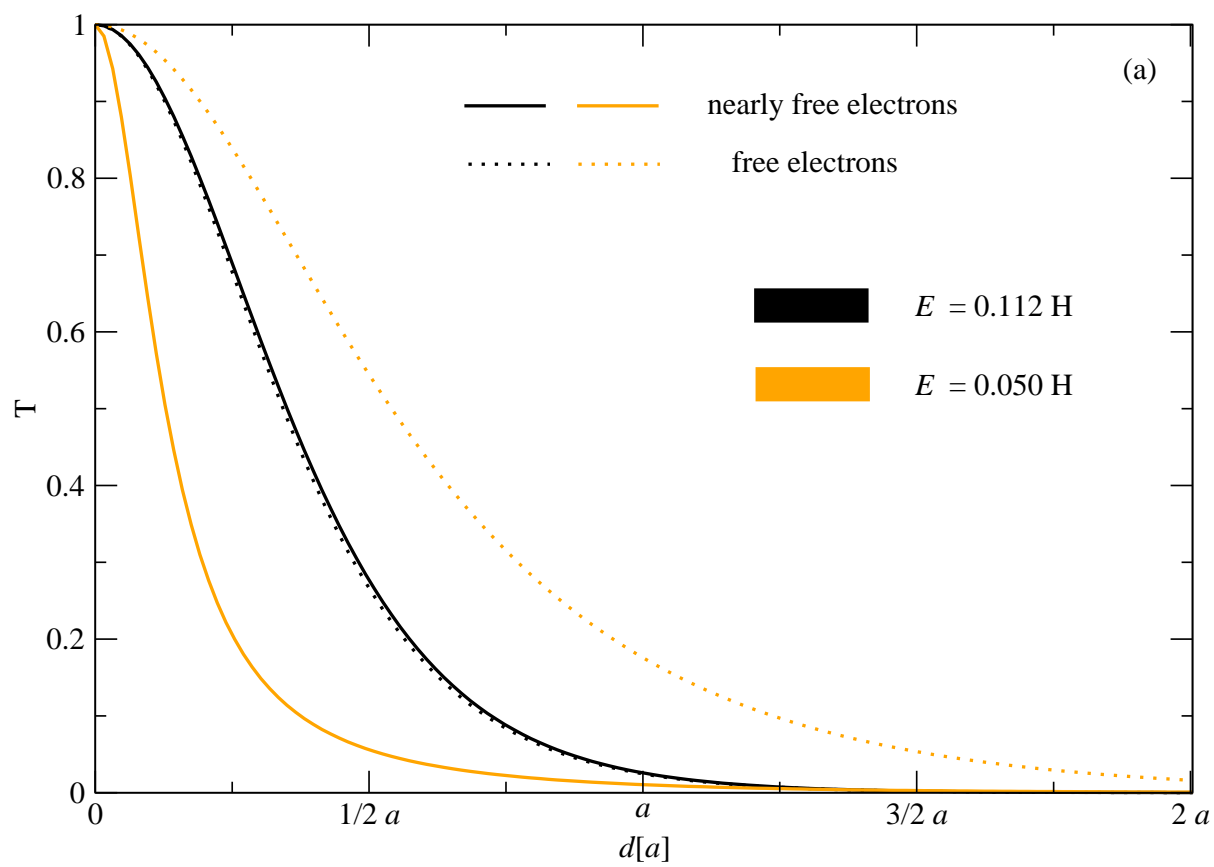
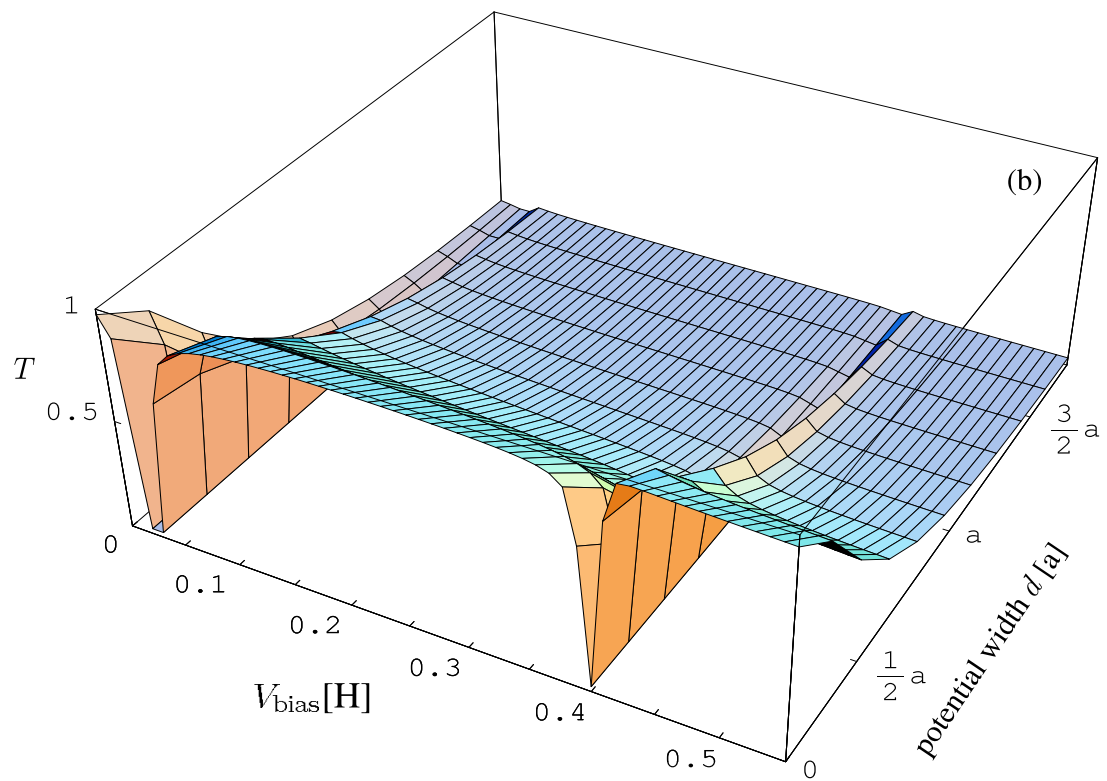


Figure 7a

Figure 7b



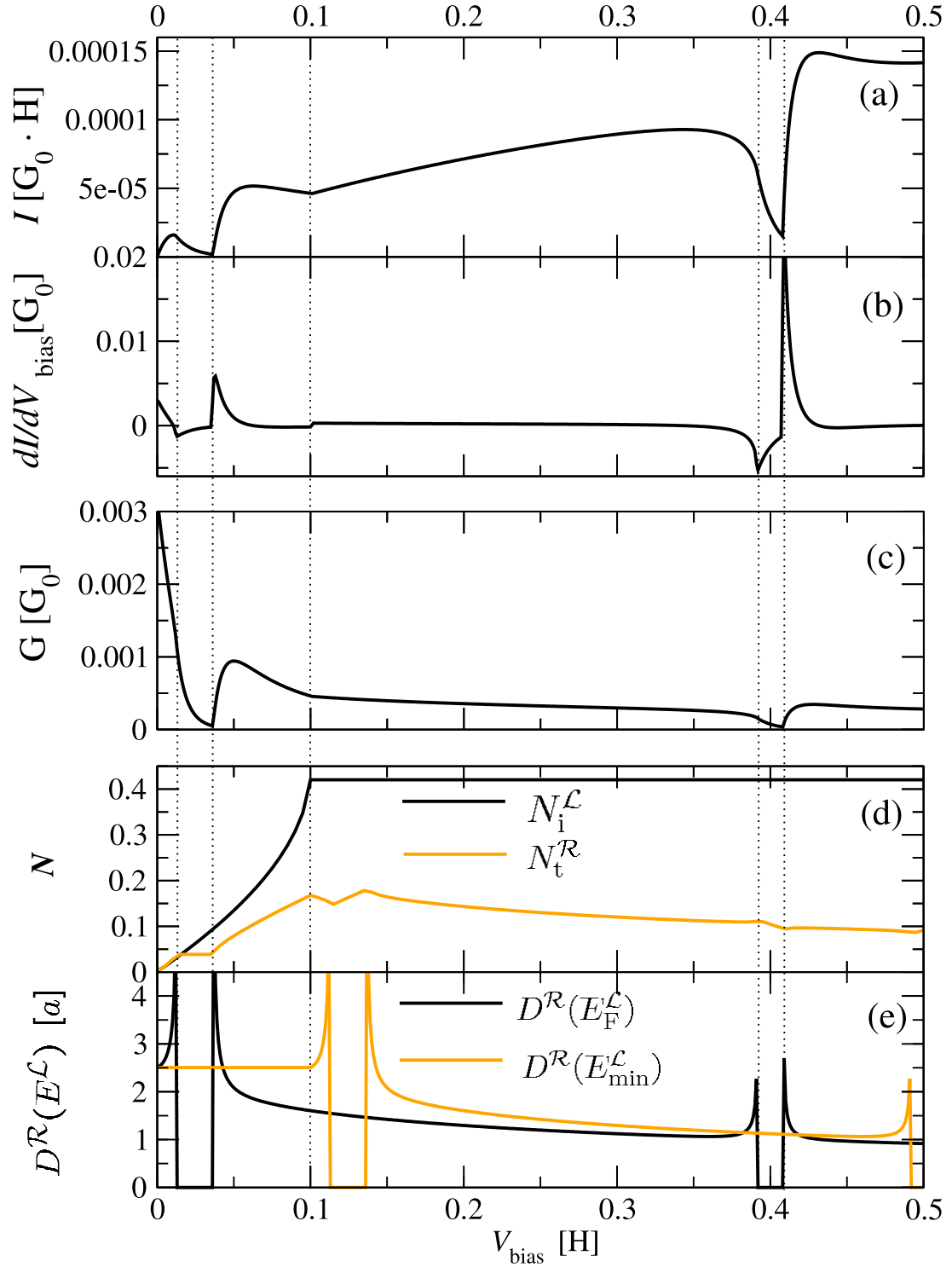


Figure 8

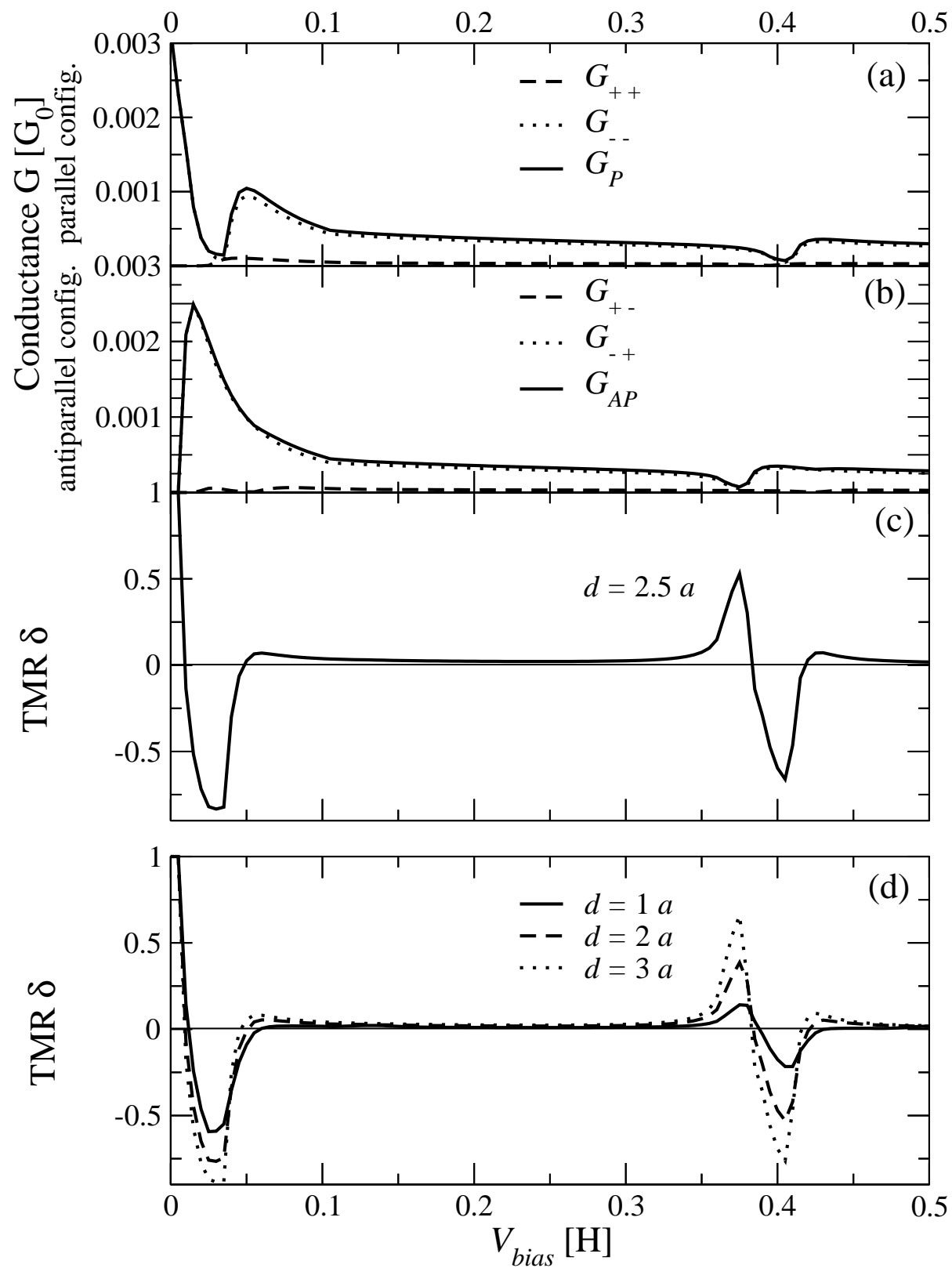


Figure 9